Inorg. Chem. **2007**, *46*, 2080–2093

Effects of Benzoannulation and α-Octabutoxy Substitution on the Photophysical Behavior of Nickel Phthalocyanines: A Combined Experimental and DFT/TDDFT Study

Alexandra V. Soldatova,[⊥] Junhwan Kim,[‡] Xinzhang Peng,[‡] Angela Rosa,*[,§] Giampaolo Ricciardi,*[,§] Malcolm E. Kenney,*[,‡] and Michael A. J. Rodgers*[,⊥]

Center for Photochemical Sciences and Department of Chemistry, Bowling Green State University, Bowling Green, Ohio 43403, Department of Chemistry, Case Western Reserve University, Cleveland, Ohio 44106, and Dipartimento di Chimica, Università della Basilicata, Via N. Sauro 85, 85100 Potenza, Italy

Received August 11, 2006

The photophysical properties of a group of Ni(II)-centered tetrapyrroles have been investigated by ultrafast transient absorption spectrometry and DFT/TDDFT methods in order to characterize the impacts of α-octabutoxy substitution and benzoannulation on the deactivation pathways of the $S_1(\pi,\pi^*)$ state. The compounds examined were NiPc, NiNc, $NiPc(OBu)_8$, and $NiNc(OBu)_8$, where Pc = phthalocyanine and Nc = naphthalocyanine. It was found that the $S_1(\pi,\pi^*)$ state of $NiNc(OBu)_8$ deactivated within the time resolution of the instrument (200 fs) to a vibrationally hot $T_1(\pi,\pi^*)$ state. The quasidegeneracy of the $S_1(\pi,\pi^*)$ and $^3(d_{z^2},d_{x^2-y^2})$ states allowed for fast intersystem crossing (ISC) to occur. After vibrational relaxation (ca. 2.5 ps), the $T_1(\pi,\pi^*)$ converted rapidly (ca. 19 ps lifetime) and reversibly into the $^3LMCT(\pi,d_{x^2-y^2})$ state. The equilibrium state, so generated, decayed to the ground state with a lifetime of ca. 500 ps. Peripheral substitution of the Pc ring significantly modified the photodeactivation mechanism of the $S_1(\pi,\pi^*)$ by inducing substantial changes in the relative energies of the $S_1(\pi,\pi^*)$, $^3(d_{\pi},d_{x^2-y^2})$, $^3(d_{z^2},d_{x^2-y^2})$, $T_1(\pi,\pi^*)$, and $^{1,3}LMCT(\pi,d_{x^2-y^2})$ excited states. The location of the Gouterman LUMOs and the unoccupied metal level ($d_{x^2-y^2}$) with respect to the HOMO is crucial for the actual position of these states. In NiPc, the $S_1(\pi,\pi^*)$ state underwent ultrafast (200 fs) ISC into a hot (d,d) state. Vibrational cooling (ca. 20 ps lifetime) resulted in a cold ($d_{z^2},d_{x^2-y^2}$) state, which repopulated the ground state with a 300 ps lifetime. In $NiPc(OBu)_8$, the $S_1(\pi,\pi^*)$ state deactivated through the $^3(d_{z^2},d_{x^2-y^2})$, which in turn converted to the $^3LMCT(\pi,d_{x^2-y^2})$ state, which finally repopulated the ground state with a lifetime of 640 ps. Insufficient solubility of NiNc in noncoordinating solvents prevented transient absorption data from being obtained for this compound. However, the TDDFT calculations were used to make speculations about the photoproperties.

Introduction

Metallophthalocyanines (MPcs) have a range of potential applications in high-tech fields, including molecular electronics, nonlinear optics, liquid crystals, and photovoltaic solar cells.[1,2] Moreover, owing to their intense near-IR absorptions within the therapeutic window where tissue absorption and scattering is minimal, metallophthalocyanines have been employed as photodynamic and photothermal sensitizers for tumor therapy and other medical applications, including photodiagnostics.[3−5]

The nature of the coordinated metal plays a central role in determining the excited-state dynamics of MPcs. For instance, metallophthalocyanines containing metal ions with

* To whom correspondence should be addressed. E-mail: rosa@unibas.it (A.R.), rg010sci@unibas.it (G.R.), malcolm.kenney@case.edu (M.E.K.), rodgers@bgnet.bgsu.edu (M.A.J.R.).
[⊥] Bowling Green State University.
[‡] Case Western Reserve University.
[§] Università della Basilicata.

(1) Wagner, R. W.; Lindsey, J. S.; Seth, J.; Palaniappan, V.; Bocian, D. F. *J. Am. Chem. Soc.* **1996**, *118*, 3996.
(2) *Phthalocyanines: Properties and Applications*; Leznoff, C. C., Lever, A. B. P., Eds.; VCH Publishers: New York, 1990−1996; Vols. 1−4.
(3) Fernández, D. A.; Awruch, J.; Dicelio, L. E. *Photochem. Photobiol.* **1996**, *63*, 784.
(4) Lawrence, D. S.; Whitten, D. G. *Photochem. Photobiol.* **1996**, *64*, 923.
(5) Szacilowski, K.; Macyk, W.; Drzawiecka-Matuszek, A.; Brindell, M.; Stochel, G. *Chem. Rev.* **2005**, *105*, 2647.

10.1021/ic061524o CCC: $37.00
Published on Web 02/15/2007

d^0 or d^{10} configurations (closed-shell) are generally fluorescent, showing significant quantum yields of long-lived triplet states.[6,7] On the other hand, complexes with open-shell central metals, such as Ni(II), Co(II), Fe, and others,[8−10] are nonluminescent. In these complexes, emission is not observed because rapid radiationless decay of the primary excited $S_1(\pi,\pi^*)$ state into low-lying (d,d) and/or MLCT/LMCT states occurs, from whence the ground-state surface can readily be reached. In these cases, rapid conversion of electronic energy into vibrational modes of the ground state is achieved, generating highly localized thermal effects that, in tissue environments, can lead to cell death.[10]

Recently, Ni(II)5,9,14,18,23,27,32,36-octabutoxy-2,3-naphthalocyanine, $NiNc(OBu)_8$,[11] has been found to meet the conditions for effective photothermal photosensitization, namely, it shows efficient photon absorption ($\epsilon_{845nm} \sim 2 \times 10^5\ M^{-1}\ cm^{-1}$) in the near-IR region where light penetrates tissues more effectively and the photogenerated excited states decay rapidly. There are now indications that this compound, being efficiently taken up by amelanotic melanoma cells, is able to effectively destroy such cells by photothermal sensitization without any requirement of molecular oxygen.[12,13]

An understanding of the factors governing the efficiency of the photothermal behavior of $NiNc(OBu)_8$ and related compounds requires knowledge of their excited-state dynamics. A combined experimental and theoretical investigation of the photophysics of the Ni(II)1,4,8,11,15,18,22,25-octabutoxyphthalocyanine, $NiPc(OBu)_8$, in toluene solution was published recently.[10] In that compound, the primary excited $S_1(\pi,\pi^*)$ state deactivates via lower-lying $^3(d_{z^2},d_{x^2-y^2})$ and $^3LMCT(\pi,d_{x^2-y^2})$ states, from whence ground-state repopulation occurs with a lifetime of 640 ps. The deactivation mechanism proposed for $NiPc(OBu)_8$ does not necessarily apply to $NiNc(OBu)_8$, as the chemical changes in the macrocycle are expected to have significant impact on the excited-state pattern and energies. For instance, the $^3(d_{z^2},d_{x^2-y^2})$, which, in $NiPc(OBu)_8$, was found to intervene only at the early stage of the decay process, might not be involved at all in the radiationless decay of $NiNc(OBu)_8$ due to the significant energy lowering (ca. 200 meV) of the primary excited $S_1(\pi,\pi^*)$ state.[11]

In the present work, the spectral and dynamic behaviors of NiPc, NiNc, $NiPc(OBu)_8$, and $NiNc(OBu)_8$ have been investigated using femtosecond transient absorption spectrometry and density functional (DFT) and time-dependent DFT (TDDFT) methods in an attempt to independently characterize the effects of the α-octabutoxy substitution and benzoannulation on the nature and rates of the deactivation pathways.

Scheme 1. Synthetic Routes Used for NiNc and $NiNc(5,36\text{-}OBu)_8$

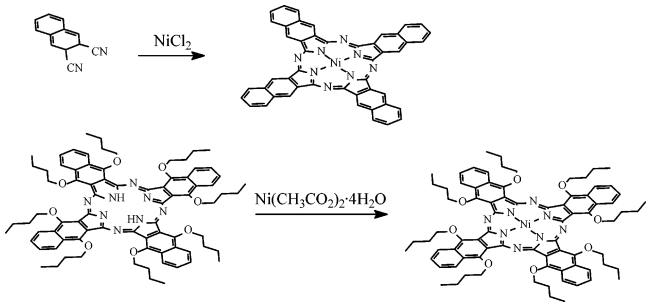

Experimental Section

A. Materials. The solvents toluene (99.5+%, spectrophotometric grade, Aldrich) and 1-chloronaphthalene (90%, technical grade, Aldrich) were used without further purification. NiPc was purchased from Aldrich Chemical Co. $NiPc(OBu)_8$ was prepared as previously described.[10] NiNc and $NiNc(OBu)_8$ were synthesized as follows (Scheme 1).

1. NiNc. The synthesis used for NiNc is a conventional cyclization and has been reported briefly before.[14] A mixture of 2,3-dicyanonaphthalene (950 mg), $NiCl_2$ (250 mg), and $(NH_4)_2MoO_4$ (2 mg) was heated (250 °C) for 3 h. The reaction product was extracted (Soxhlet extractor) with benzene for 20 h, CH_3OH for 6 h, and dimethylformamide for 60 h. It then was heated (80 °C) with aqueous NaOH (10%, 20 mL) for 1 h, heated (80 °C) with aqueous HCl (10%, 20 mL) for 1 h, dissolved in H_2SO_4 (concentrated, 6 mL), and recovered by dilution of the solution with H_2O (30 mL). Finally, it was washed (H_2O, acetone), vacuum dried (100 °C), and weighed (400 mg, 39%). UV−vis (1-chloronaphthalene) λ_{max}, nm: 770. The compound is a green solid. It is insoluble in CH_2Cl_2, dimethylformamide, toluene, and hexanes. The insolubility of this compound in organic solvents precludes its purification by chromatography.

2. $NiNc(5,36\text{-}OBu)_8$. Under Ar, a refluxing solution of $H_2Nc(5,36\text{-}OBu)_8$ (134 mg), 1,8-diazabicyclo[5.4.0]undec-7-ene (0.02 mL), and 1-butanol (3 mL) was treated with 10 portions of $Ni(CH_3CO_2)_2{\cdot}4H_2O$ (154 mg) over 3 days, diluted with a solution of CH_3OH and H_2O (1:1, 6 mL), and filtered. The solid was chromatographed (Al_2O_3(III), toluene), vacuum dried (room temperature), and weighed (88 mg, 63%). UV−vis (toluene) λ_{max}, nm (log ϵ): 844 (5.5). NMR ($CDCl_3$): δ 8.93 (m, 8H, 1,4-Nc H), 7.86 (m, 8H, 2,3-Nc H), 5.03 (t, 16H, OCH_2), 2.20 (m, 16H, OCH_2CH_2), 1.65 (m, 16H, $OC_2H_4CH_2$), 1.03 (t, 24H, $OC_3H_6CH_3$). HRMS−ESI−TOF *m/z*: $[M]^+$ calcd for $C_{80}H_{88}N_8O_8{}^{58}Ni$, 1346.6079; found, 1346.6073. The compound is a green solid. It is soluble in CH_2Cl_2, dimethylformamide, and toluene and is slightly soluble in hexanes.

B. UV−Visible Absorption Spectra. The ground-state electronic absorption spectra were recorded at room temperature on a Varian Cary 50 Bio (Varian Corporation) UV−visible single-beam spectrophotometer using a 10 or 2 mm path length quartz cuvette.

(6) Rihter, B. D.; Kenney, M. E.; Ford, W. E.; Rodgers, M. A. J. *J. Am. Chem. Soc.* **1993**, *115*, 8146.
(7) Kobayashi, N.; Ogata, H.; Nonaka, N.; Luk'yanets, E. A. *Chem.—Eur. J.* **2003**, *9*, 5123.
(8) Ishii, K.; Kobayashi, N. In *The Porphyrin Handbook*; Kadish, K. M., Smith, K. M., Guilard, R., Eds.; Academic Press: New York, 2003.
(9) Lecomte, C.; Rohmer, M. M.; Benard, M. In *The Porphyrin Handbook*; Kadish, K. M., Smith, K. M., Guilard, R., Eds.; Academic Press: New York, 2003.
(10) Gunaratne, T. C.; Gusev, A. V.; Peng, X.; Rosa, A.; Ricciardi, G.; Baerends, E. J.; Rizzoli, C.; Kenney, M. E.; Rodgers, M. A. J. *J. Phys. Chem. A* **2005**, *109*, 2078.
(11) Busetti, A.; Soncin, M.; Reddi, E.; Rodgers, M. A. J.; Kenney, M. E.; Jori, G. *J. Photochem. Photobiol., B* **1999**, *53*, 103.
(12) Camerin, M.; Rello, S.; Villaneuva, A.; Ping, X.; Kenney, M. E.; Rodgers, M. A. J.; Jori, G. *Eur. J. Cancer* **2005**, *41*, 1203.
(13) Camerin, M.; Rodgers, M. A. J.; Kenney, M. E.; Jori, G. *Photochem. Photobiol. Sci.* **2005**, *4*, 251.
(14) Mikhalenko, S. A.; Luk'yanets, E. A. *Zh. Obshch. Khim.* **1969**, *39*, 2554−2558; *J. Gen. Chem. USSR (Engl. Transl.)* **1969**, *39*, 2495.

C. Ultrafast Pump−Probe Measurements. Details of the pump−probe instrument for ultrafast transient absorption measurements at the Ohio Laboratory for Kinetic Spectrometry at Bowling Green State University have been described previously.[15] The recent improvements to enhance signal-to-noise characteristics have been published elsewhere.[16] For the present measurements, the main part (95%) of the fundamental output beam (95 fs, 1 kHz, 800 nm) from an amplified, mode-locked Ti:sapphire laser (Hurricane, Spectra-Physics) was used to excite the sample or to pump an optical parametric amplifier (OPA 800, Spectra-Physics) to generate excitation pulses in the 330−845 nm region. The pump intensity was attenuated to have an energy of 1−6 μJ per pulse at the sample. The linear polarization of the pump beam was set at the magic angle (54.7°) with respect to that of the probe beam in order to eliminate any temporal components arising from molecular rotations. The transient absorption signal was monitored with the white-light continuum probe in the spectral range of 460−780 nm or with the extended to the near-IR continuum in the region of 800−1100 nm. The instrument response time of the ultrafast spectrometer was ca. 200 fs. The absorption spectra of the solutions were measured before and after the experiment to check for possible sample degradation.

D. Quantum Chemical Calculations. All calculations have been performed with the ADF (Amsterdam Density Functional) suite of programs, release 2004.01.[17,18] The calculations made use of the local density approximation (LDA) functional of Vosko−Wilk−Nusair (VWN)[19] plus the generalized gradient approximation (GGA), employing Becke's[20] gradient approximation for exchange and Perdew's[21] approximation for correlation (BP). The excitation energies were calculated using time-dependent density functional theory (TDDFT). In the ADF implementation,[22,23] the solution of the TDDFT response equations proceeds in an iterative fashion starting from the usual ground-state or zeroth-order Kohn−Sham (KS) equations.[23] For these, one needs an approximation to the usual static exchange-correlation (xc) potential, $v_{xc}(\mathbf{r})$. After the ordinary KS equations have been solved, the first-order density change has to be calculated from an iterative solution to the first-order KS equations. In these first-order equations, an approximation is needed to the first functional derivative of the time-dependent xc potential, $v_{xc}(\mathbf{r}, t)$, with respect to the time-dependent density $\rho(\mathbf{r}', t')$, the so-called xc kernel. For the xc kernel, we used the adiabatic local density approximation (ALDA). In this approximation, the time dependence (or frequency dependence, referring to the Fourier-transformed kernel) is neglected, and one simply uses the differentiated static LDA expression. In our case, the Vosko−Wilk−Nusair parametrization was used.[19] For the exchange-correlation potentials, which appear in the zeroth-order KS equations, we employed the same GGA as that in the DFT calculations.

Table 1. Selected Bond Distances (Å) and Bond Angles (deg) Calculated for NiPc, NiNc, NiPc(OMe)$_8$, and NiNc(OMe)$_8$. X-ray Data Are in Italics

	NiPc D_{4h}	NiNc D_{4h}	NiPc(OMe)$_8$ D_{2d}	NiNc(OMe)$_8$ D_{2d}
Ni−N$_p$	1.912	1.917	1.900	1.906
	1.887(6)[a]	*1.929(7)*[b]	*1.878(4)*[c]	
C$_\alpha$−N$_p$	1.384	1.384	1.382	1.381
	1.379(12)		*1.376(6)*	
C$_\alpha$−C$_\beta$	1.452	1.451	1.453	1.453
	1.456(7)		*1.455(7)*	
C$_\beta$−C$_\beta$	1.402	1.416	1.406	1.430
	1.292(10)		*1.397(7)*	
C$_\alpha$−N$_b$	1.318	1.317	1.319	1.320
	1.320(9)		*1.320(6)*	
C$_o$−O			1.363	1.368
			1.361(6)	
C$_\alpha$−N$_p$−C$_\alpha$	106.9	107.2	107.5	107.6
	110.6(14)		*107.0(4)*	
C$_\alpha$−N$_\beta$−C$_\alpha$	121.3	121.4	121.2	122.2
	119.2(6)		*120.1(4)*	
O···O			3.793	3.865
			3.910(2)	
C$_{Me}$−O−C$_o$−C$_\beta$			177.4	63.0
(C$_\alpha$−N$_p$−N$_p$−C$_\alpha$)$_{ad}$[d]	0.0	0.0	12.5	11.3
			16.2(4)	

[a] X-ray data for NiPcI; from ref 25. [b] From ref 28. [c] X-ray data for NiPc(OBu)$_8$; from ref 10. [d] Dihedral angle (deg) between adjacent pyrrole ring planes.

To facilitate the calculations, the butyl substituents were replaced by methyl groups.

In all of the DFT and TDDFT calculations, the all-electron ADF TZ2P basis set, which is an uncontracted, triple-ζ STO basis set with one 3d and one 4f polarization function for C, N, and O atoms, one 2p and one 3d polarization function for H, and a triple-ζ 3d, 4s basis with one 4p and one 4f function for Ni, was used.

The vertical absorption energies, E_{va}, have been evaluated at the ground-state optimized geometry. The adiabatic energies, E_{adia}, have been obtained according to the expression

$$E_{adia} = E_{ve} + \Delta E$$

where E_{ve} is the vertical emission energy, which is calculated at the TDDFT level using the relaxed excited-state geometry. The ΔE term accounts for the change in energy of the ground state upon deformation to the relaxed geometry of the excited state (for a schematic definition of the calculated energies, see Figure 10 in ref 10).

Geometry optimizations were performed for the ground and selected triplet excited states of the complexes of the series. Open-shell DFT calculations for the triplet states were performed within a spin-unrestricted formalism, and spin contamination, monitored by the expectation value of $\mathbf{S}^2$, was found to be negligible. The optimized ground-state and excited-state structures were verified to be true minima by frequency calculations.

Results and Discussion

A. Ground-State Molecular and Electronic Structure. In this section, the molecular and electronic structure effects of introducing benzo rings and alkoxy groups at the α-position both separately and together into the basic Pc structure are examined.

The most relevant geometrical parameters calculated for NiPc, NiNc, NiPc(OMe)$_8$, and NiNc(OMe)$_8$ are gathered in Table 1 and compared to the available experimental data. The molecular structure of NiPc has been investigated

(15) Nikolaitchik, A. V.; Korth, O.; Rodgers, M. A. J. *J. Phys. Chem. A* **1999**, *103*, 7587.
(16) Pelliccioli, A. P.; Henbest, K.; Kwag, G.; Carvagno, T. R.; Kenney, M. E.; Rodgers, M. A. J. *J. Phys. Chem. A* **2001**, *105*, 1757.
(17) *Amsterdam Density Functional Program*; Theoretical Chemistry, Vrije Universiteit: Amsterdam, The Netherlands. http://www.scm.com.
(18) te Velde, G.; Bickelhaupt, F. M.; Baerends, E. J.; Fonseca Guerra, C.; van Gisbergen, S. J. A.; Snijders, J. G.; Ziegler, T. *J. Comput. Chem.* **2001**, *22*, 931.
(19) Vosko, S. H.; Wilk, L.; Nusair, M. *Can. J. Phys.* **1980**, *58*, 1200.
(20) Becke, A. *Phys. Rev. A* **1988**, *38*, 3098.
(21) Perdew, J. P. *Phys. Rev. B* **1986**, *33*, 8822 (Erratum: *Phys. Rev. B* **1986**, *34*, 7406).
(22) van Gisbergen, S. J. A.; Snijders, J. G.; Baerends, E. J. *Comput. Phys. Commun.* **1999**, *118*, 119.
(23) van Gisbergen, S. J. A.; Snijders, J. G.; Baerends, E. J. *J. Chem. Phys.* **1995**, *103*, 9347.

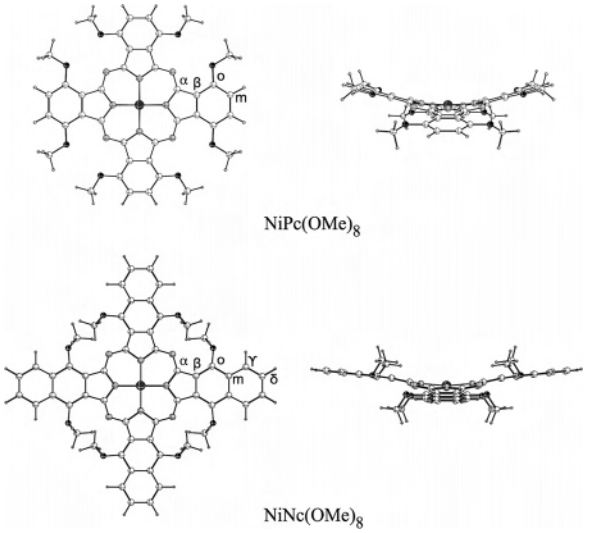

Figure 1. Top view (left) and side view (right) of the DFT-optimized molecular structures of $NiPc(OMe)_8$ and $NiNc(OMe)_8$.

extensively both experimentally[24−26] and theoretically,[26,27] and a planar D_{4h} structure is, by now, well-established for this complex. According to the crystallographic data by Araki et al.,[28] the linearly benzoannulated analogue, NiNc, also possesses a planar D_{4h} structure. Experimental and theoretical structural data indicate that linear benzoannulation induces a small, although not negligible, lengthening of the $Ni-N_p$ distance (cf. Table 1).

For the α-butoxy-substituted systems, X-ray studies of $NiPc(OBu)_8$ have shown that introduction of eight butoxy groups at the α-positions induces a remarkable saddling of the phthalocyanine ring,[10] with the dihedral angle between adjacent indole rings averaging 16.2(4)°. DFT studies on the model complex $NiPc(OMe)_8$ also pointed to a D_{2d}-saddled conformation of the macrocycle (see Figure 1) both in the gas phase and in solution.[10] Therefore, it has been argued that the saddling distortion is not merely dictated by packing requirements; rather, it originates from intrinsic electronic factors such as the necessity to minimize the steric hindrance between the lone pairs of the facing oxygen atoms, while preserving an efficient nickel−phthalocyanine interaction. Indeed, as can be inferred from Table 1, the $Ni-N_p$ distance shortens significantly going from the planar NiPc to the saddled butoxy derivative.

Unfortunately, there are no X-ray structural data available for $NiNc(OBu)_8$. In spite of the numerous attempts, we were not able to grow crystals of this complex suitable for structural investigation. Geometry optimization of the model complex $NiNc(OMe)_8$ without symmetry constraint afforded the D_{2d}-saddled structure of Figure 1. This structure, which corresponds to a stable energy minimum (all-positive harmonic frequencies), shows a degree of saddling that is only slightly smaller than that computed for $NiPc(OMe)_8$ (11.3° vs 12.5°). A ruffled structure of S_4 symmetry, characterized by an up−down arrangement of the methyl groups, was also theoretically explored. However, the S_4 structure was found to be ∼12 kcal/mol less stable than the D_{2d}-saddled structure.

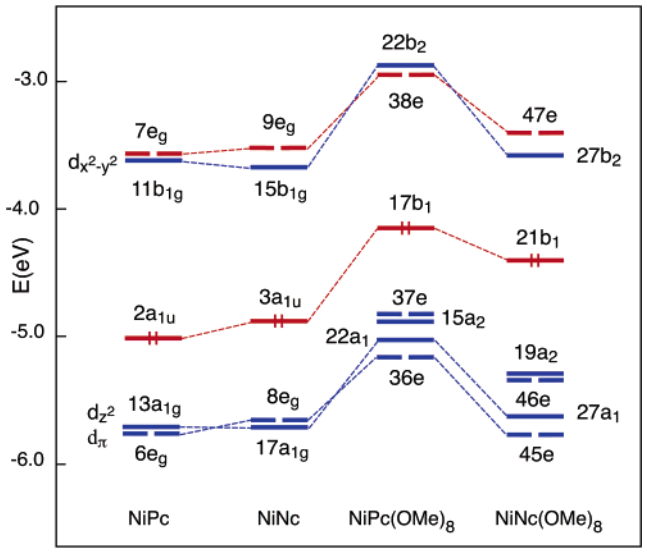

Figure 2. Energy level scheme for NiPc, NiNc, $NiPc(OMe)_8$, and $NiNc(OMe)_8$. In the numbering of the MOs, the core electrons (C, N, O, 1s; Ni, 1s−2p) are not included. For the sake of comparison with NiPc and NiNc, the unoccupied metal orbitals of $NiPc(OMe)_8$ and $NiNc(OMe)_8$, $22b_2$ and $27b_2$, respectively, are referred to as $d_{x^2-y^2}$ MOs.

It is apparent from the DFT-calculated structures of $NiPc(OMe)_8$ and $NiNc(OMe)_8$ in Figure 1 that the most striking effect of benzoannulation is the displacement of the methyl groups from the plane of the corresponding indole ring to relieve steric hindrance between the $C_{Me}-H$ and $C_\gamma-H$ σ bonds. The torsion angle $C_{Me}-O-C_o-C_\beta$, which provides a measure of the displacement of the C_{Me} atoms from the indole plane, is 63.0° in $NiNc(OMe)_8$ and 177.4° in $NiPc(OMe)_8$, where the C_{Me} atoms are nearly coplanar with the benzo rings.

The lengthening of the C_o-O bond distance going from $NiPc(OMe)_8$ to $NiNc(OMe)_8$, see Table 1, is indicative of a less effective conjugation between the oxygen lone pairs and the macrocycle π system in the naphthalocyanine. The decreased π conjugation can be traced to the tilting of the methyl groups that makes the interaction between the oxygen lone pairs and the macrocycle π system less favorable.

The highest-occupied and the lowest-unoccupied ground-state, one-electron levels of NiPc, NiNc, $NiPc(OMe)_8$, and $NiNc(OMe)_8$ are shown in Figure 2.

In our choice of the axes, the *x* and *y* axes bisect the indole rings in the planar D_{4h} structures of NiPc and NiNc and point to the *meso*-nitrogen atoms in the saddled D_{2d} structures of $NiPc(OMe)_8$ and $NiNc(OMe)_8$.

Considering, first, NiPc as a point of reference for the series, among the one-electron levels in Figure 2, one may recognize the π G-$2a_{1u}$ and the π^* G-$7e_g$ (G = Gouterman) orbitals and the metal 3d orbitals. In the virtual spectrum, there is the $3d_{x^2-y^2}$ ($11b_{1g}$), which is composed of $3d_{x^2-y^2}$ and N_p lone pairs in almost equal amount and pushed up by

(24) Robertson, J. M. *J. Chem. Soc.* **1936**, 1195.
(25) Schramm, C. J.; Scaringe, R. P.; Stojakovic, D. R.; Ibers, J. A.; Marks, T. J. *J. Am. Chem. Soc.* **1980**, *102*, 6702.
(26) Mastryukov, V.; Ruan, C.-y.; Fink, M.; Wang, Z.; Pachter, R. *J. Mol. Struct.* **2000**, *556*, 225.
(27) Rosa, A.; Ricciardi, G.; Baerends, E. J.; van Gisbergen, S. J. A. *J. Phys. Chem. A* **2001**, *105*, 3311.
(28) Morishige, K.; Araki, K. *J. Chem. Soc., Dalton Trans.* **1996**, 4303.

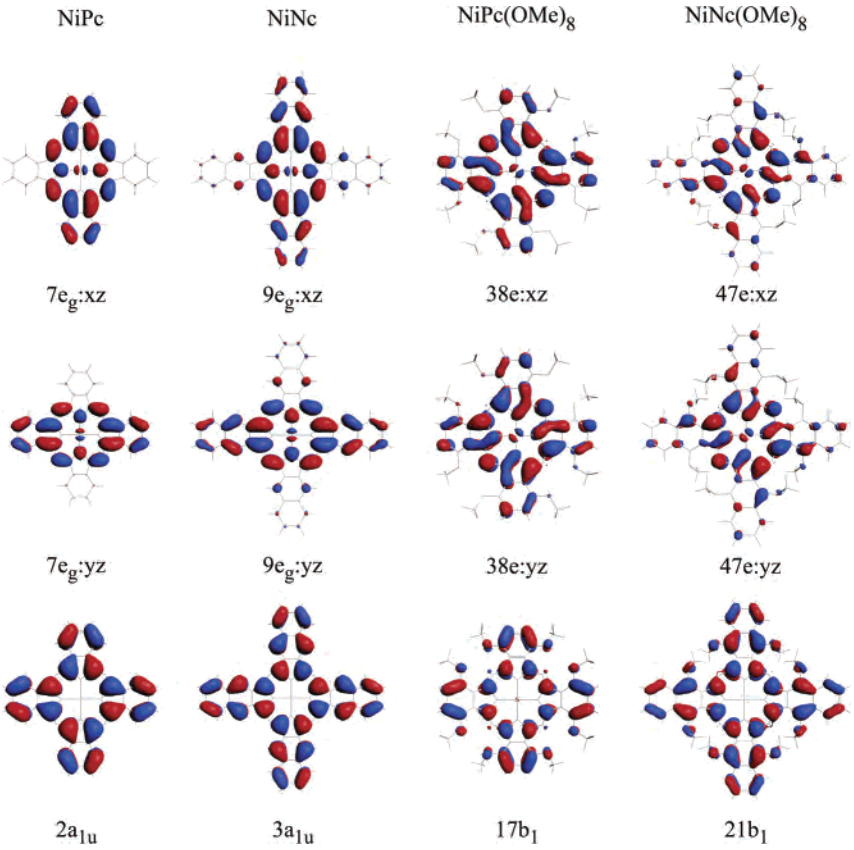

Figure 3. Visual representation of the HOMO and the pair of Gouterman LUMOs for NiPc, NiNc, $NiPc(OMe)_8$, and $NiNc(OMe)_8$.

antibonding between the $3d_{x^2-y^2}$ and the N_p lone pairs. The highest occupied 3d levels are the $3d_{z^2}$ ($13a_{1g}$), which is an almost pure metal orbital, and the $3d_\pi$ ($6e_g$). The $6e_g$ is heavily (41%) mixed with the N_p-based π orbitals of the phthalocyanine ring. (For an extensive discussion of the electronic structure of NiPc, see refs 27, 29.) According to the level pattern in Figure 2, the outstanding difference between NiP and NiNc is the destabilization of the HOMO ($3a_{1u}$). The pushing up effect of the annulated benzo rings is in accordance with the antibonding between the Pc ring system and the annulated benzo rings, which is apparent in the plot of the NiNc HOMO in Figure 3. The fused benzo rings also have some pushing up effect on the G-e_g($9e_g$) orbitals. The two degenerate $9e_g$ MOs are, however, less destabilized than the HOMO because each component of the degenerate pair feels the antibonding effect of only two of the four fused benzo rings. As for the metal states, apart from a modest stabilization of the Ni-$3d_{x^2-y^2}$ due to the slight lengthening of the Ni−N_p bond distance, their energy and composition change very little upon benzoannulation.

In a previous paper,[10] it was pointed out that the electron-releasing methoxy groups cause a destabilization of all of the levels in $NiPc(OMe)_8$. MOs with large amplitude on the *ortho*-carbons of the benzo ring are most affected, owing to the antibonding between the C_o-$2p_z$ and the oxygen lone pairs of the methoxy groups. This is the case for the $17b_1$ (HOMO) (cf. the plot of this orbital for $NiPc(OMe)_8$ in Figure 3), the 37e (HOMO−1), and the $15a_2$ (HOMO−2). Notably, the 37e and $15a_2$ are upshifted by ∼1.8 eV with respect to the equivalent orbitals ($5e_g$ and $2b_{1u}$) in NiPc (these orbitals are too low in energy to show in Figure 2).

When comparing the one-electron levels of NiNc and $NiNc(OMe)_8$ in Figure 2, it is apparent that α-alkoxy substitution of the Nc ring does not induce the generalized destabilization of the levels observed upon α-alkoxy substitution of the Pc ring. This can be explained primarily by the tilting of the methyl groups (see Figure 1) lowering the charge transfer from the electron-releasing alkoxy groups to the macrocycle. According to the Hirshfeld charge analysis, the oxygen atoms carry more negative charge in $NiNc(OMe)_8$ than in $NiPc(OMe)_8$ (0.1061 vs 0.0906 electrons). The level scheme in Figure 2 shows that the most relevant electronic effect of α-alkoxy substitution of the Nc ring consists of the upshift of the $3a_1$-derived $21b_1$ (HOMO) induced by the antibonding (Figure 3) between the Nc-$3a_{1u}$, which has large amplitude (28%) on the *ortho*-carbons (C_o), and the oxygen lone pairs of the methoxy groups whose contribution to this orbital is approximately 6%. The α-methoxy substitution also lifts two low-lying NiNc levels, the $7e_g$ and $3b_{1u}$ (not shown in the diagram in Figure 2), which become the HOMO−1 ($19a_2$) and the HOMO−2 (46e) of $NiNc(OMe)_8$. The empty G orbitals, the 47e, although having appreciable amplitude (∼10%) on the *ortho*-carbons, are destabilized very little due to the minor (∼1%) contribution of the oxygen lone pairs. The important consequence is that the energy gap between the HOMO and the pair of unoccupied Gouterman orbitals diminishes considerably going from NiNc to $NiNc(OMe)_8$.

(29) Rosa, A.; Baerends, E. J. *Inorg. Chem.* **1994**, *33*, 584.

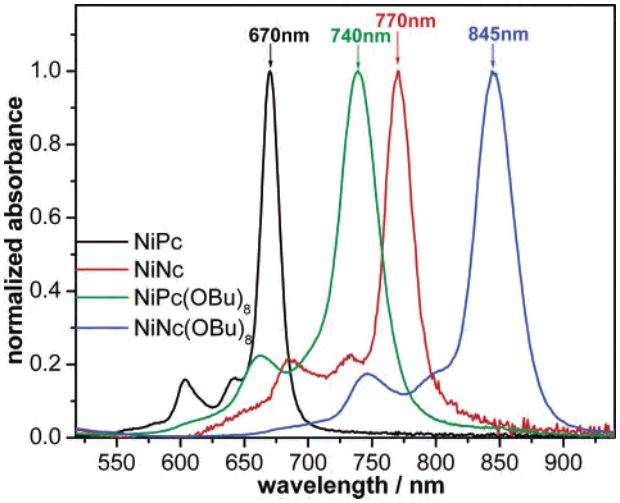

Figure 4. Normalized ground-state absorption spectra of NiPc, NiNc, $NiPc(OBu)_8$, and $NiNc(OBu)_8$ in 1-chloronaphthalene at room temperature.

Table 2. Vertical Excitation Energies and Oscillator Strengths (*f*) Computed for the Optically Allowed Excited States Responsible for the Q Band

	TDDFT				Expt
	state	composition (%)	E_{va} (eV/nm)	*f*	*E* (nm)
NiPc	1^1E_u	$2a_{1u} \rightarrow 7e_g$ (93)	1.98/627	0.588	670[a]
NiNc	1^1E_u	$3a_{1u} \rightarrow 9e_g$ (94)	1.61/770	0.742	770[a]
$NiPc(OMe)_8$[b]	1^1E	$17b_1 \rightarrow 38e$ (91)	1.60/775	0.513	740,[a] 734[c]
	1^1B_2	$37e \rightarrow 38e$ (92)	2.02/614	0.012	
	3^1E	$15a_2 \rightarrow 38e$ (92)	2.07/599	0.357	
$NiNc(OMe)_8$	1^1E	$21b_1 \rightarrow 47e$ (94)	1.38/898	0.658	845,[a] 845[d]
	3^1E	$19a_2 \rightarrow 47e$ (86)	1.98/627	0.302	
	1^1B_2	$46e \rightarrow 47e$ (84)	2.01/617	0.007	

[a] Data taken in 1-chloronaphthalene at room temperature; this work. [b] Theoretical data from ref 10. [c] Data taken in toluene at room temperature; ref 10. [d] Data taken in toluene at room temperature; this work.

From the level scheme in Figure 2, it may be inferred that the relative position of the Gouterman LUMOs and that of the unoccupied metal level ($d_{x^2-y^2}$) with respect to the HOMO changes significantly along the series. This is crucial for the photophysical properties (vide infra).

B. Excited States. 1. Ground-State Absorption Spectra. The normalized ground-state absorption spectra of the complexes, in the energy window of interest, are displayed in Figure 4. The spectra show a red shift of the intense Q(0,0) band upon either benzoannulation (100 nm shift) or octabutoxy substitution (70 nm shift). The Q(0,0) band of $NiNc(OBu)_8$, where the effects of the benzoannulation and α-butoxy substitution are both operative, is red shifted by ~170 nm relative to that of NiPc. Looking at the overlaid spectra in Figure 4, it is apparent that α-butoxy substitution of both the Pc and Nc rings also induces a substantial broadening of the Q bands, a feature that can be linked to the conformational flexibility of the peripheral butoxy groups.

An interpretation of the spectral changes observed along the series is provided by TDDFT calculations of the lowest optically allowed excited states. According to the vertical absorption energies (E_{va}) and oscillator strengths gathered in Table 2, the intense Q(0,0) band is invariably assigned to the lowest optically allowed excited state (1^1E_u for NiPc and NiNc, 1^1E for the α-alkoxy-substituted systems). The calculated excitation energies are in satisfactory agreement with the experiment, with the Q(0,0) λ_{max} being underestimated by no more than 0.13 eV (NiPc). However, the discrepancy between theory and experiment varies from one compound to another such that the Q-band maxima of NiNc and $NiPc(OMe)_8$, which are only 30 nm apart, are predicted at nearly the same energy. The composition of the BP/ALDA solution vectors, in terms of the major one-electron MO transitions reported in Table 2, indicates that, in all complexes, the Q state is largely derived from promotion of one electron from the HOMO to the degenerate pair of unoccupied Gouterman MOs. The increasingly reduced energy gap between these orbitals along the series (see Figure 2) fits in with the observed shift of the Q(0,0) band to longer wavelengths. In the energy regime of the Q bands, a second, intense excited state, the 3^1E, is predicted for the α-alkoxy-substituted systems. This state, computed at 2.07 eV (599 nm) in $NiPc(OMe)_8$ and at 1.98 (627 nm) in $NiNc(OMe)_8$, contributes to the broadening of the blue side of the Q-band system.

Table 3. Excitation Energies (eV), Composition, and Character of the Lowest Excited States of NiPc and NiNc

state	composition (%)	character	E_{va}	E_{adia}
	NiPc			
1^3A_{2g}	$6e_g \rightarrow 7e_g$ (100)	MLCT	2.08	
1^3B_{2g}	$6e_g \rightarrow 7e_g$ (100)	MLCT	2.02	
1^1E_u	$2a_{1u} \rightarrow 7e_g$ (93)	π,π^*	1.98	
1^3A_{1g}	$6e_g \rightarrow 7e_g$ (100)	MLCT	1.98	
1^3E_g	$6e_g \rightarrow 11b_{1g}$ (99)	$d_\pi, d_{x^2-y^2}$	1.77	1.56 (1^3B_{3g})[a]
1^3B_{1g}	$13a_{1g} \rightarrow 11b_{1g}$ (100)	$d_{z^2}, d_{x^2-y^2}$	1.62	1.34[b]
1^1B_{1u}	$2a_{1u} \rightarrow 11b_{1g}$ (100)	LMCT	1.47	1.30[b,c]
1^3B_{1u}	$2a_{1u} \rightarrow 11b_{1g}$ (100)	LMCT	1.45	1.29[b]
1^3E_u	$2a_{1u} \rightarrow 7e_g$ (100)	π,π^*	1.37	1.30 (1^3A_u)[d]
	NiNc			
1^3B_{2g}	$3a_{1u} \rightarrow 5b_{2u}$ (97)	π,π^*	1.85	
1^3E_g	$8e_g \rightarrow 15b_{1g}$ (89)	$d_\pi, d_{x^2-y^2}$	1.71	1.52(1^3B_{3g})[a]
1^1E_u	$3a_{1u} \rightarrow 9e_g$ (94)	π,π^*	1.61	
1^3B_{1g}	$17a_{1g} \rightarrow 15b_{1g}$ (100)	$d_{z^2}, d_{x^2-y^2}$	1.58	1.30[b]
1^3E_u	$3a_{1u} \rightarrow 9e_g$ (100)	π,π^*	1.10	1.05 (1^3A_u)[e]
1^1B_{1u}	$3a_{1u} \rightarrow 15b_{1g}$ (100)	LMCT	1.05	0.90[b,c]
1^3B_{1u}	$3a_{1u} \rightarrow 15b_{1g}$ (100)	LMCT	1.04	0.89[b]

[a] The energy values refer to the Jahn−Teller-distorted rectangular D_{2h} structures. [b] The energy values refer to the structures optimized under the D_{4h} symmetry constraint. [c] Computed at the optimized geometry of the corresponding triplet. [d] The energy value refers to the Jahn−Teller-distorted C_{2h} structure. [e] The energy value refers to the Jahn−Teller-distorted C_i structure.

2. Optically Silent Excited States Below the $S_1(\pi,\pi^*)$ State. In order to provide a theoretical basis for the interpretation of the deactivation mechanism of the $S_1(Q)$ state along the investigated series, we have examined the lowest singlet and triplet excited states of NiPc, NiNc, $NiPc(OMe)_8$, and $NiNc(OMe)_8$. The vertical absorption energies (E_{va}) calculated for the whole set of singlet and triplet states up to ~0.3 eV above the $S_1(Q)$ state are gathered in Tables 3 and 4, together with the adiabatic energies (E_{adia}) calculated for selected states. In Figure 5, these selected excited states are plotted for all investigated compounds, for the sake of comparison.

Considering first NiPc, the TDDFT results in Table 3 indicate that five dark states lie vertically below the $S_1(\pi,\pi^*)$

Table 4. Excitation Energies (eV), Composition, and Character of the Lowest Excited States of NiPc(OMe)$_8$ and NiNc(OMe)$_8$

state	composition (%)	character	E_{va}	E_{adia}
		NiPc(OMe)$_8$[a]		
2^3A_2	37e → 38e (100)	π,π^*	1.88	
1^3B_1	37e → 38e (100)	π,π^*	1.86	
2^3B_2	37e → 38e (100)	π,π^*	1.83	
2^3E	37e → 22b$_2$ (78)	LMCT/d_π,$d_{x^2-y^2}$	1.83	
	36e → 22b$_2$ (22)			
1^3B_2	22a$_1$ → 22b$_2$ (98)	d_{z^2},$d_{x^2-y^2}$	1.69	1.39[b]
1^1E	17b$_1$ → 38e (91)	π,π^*	1.60	
1^1A_2	17b$_1$ → 22b$_2$ (100)	LMCT	1.28	1.15[b,c]
1^3A_2	17b$_1$ → 22b$_2$ (100)	LMCT	1.27	1.13[b]
1^3E	17b$_1$ → 38e (100)	π,π^*	1.15	1.09 (1^3B_2)[d]
		NiNc(OMe)$_8$		
1^3B_2	27a$_1$ → 27b$_2$ (100)	d_{z^2},$d_{x^2-y^2}$	1.63	1.31[b]
2^3E	46e → 27b$_2$ (86)	LMCT/d_π,$d_{x^2-y^2}$	1.61	
	45e → 27b$_2$ (13)			
1^1E	21b$_1$ → 47e (94)	π,π^*	1.38	
1^3E	21b$_1$ → 47e (100)	π,π^*	0.92	0.88 (1^3B_2)[d]
1^1A_2	21b$_1$ → 27b$_2$ (100)	LMCT	0.84	0.67[b,c]
1^3A_2	21b$_1$ → 27b$_2$ (100)	LMCT	0.84	0.66[b]

[a] Data from ref 10. [b] The energy values refer to the structure optimized under the D_{4h} symmetry constraint. [c] Computed at the optimized geometry of the corresponding triplet. [d] The energy values refer to the Jahn−Teller-distorted C_{2v} structures.

state. They are the 1^3E_g, 1^3B_{1g}, 1^1B_{1u}, 1^3B_{1u}, and 1^3E_u, which appear vertically at 1.77, 1.62, 1.47, 1.45, and 1.37 eV, respectively. These are the most plausible candidates as deactivation channels for the initially excited $S_1(\pi,\pi^*)$ state.

According to the BP/ALDA solution vectors in Table 3, the 1^3E_g and 1^3B_{1g} both have (d,d) character, being described by the $6e_g \rightarrow 11b_{1g}$ ($d_\pi \rightarrow d_{x^2-y^2}$) and $13a_{1g} \rightarrow 11b_{1g}$ ($d_{z^2} \rightarrow d_{x^2-y^2}$) transitions, the 1^3E_u is the normally emissive $T_1(\pi,\pi^*)$ state, and the $1^{1,3}B_{1u}$ are pure $2a_{1u} \rightarrow 11b_{1g}$ LMCT states.[30−35] As inferred from the data in Table 3, the adiabatic energies of the LMCT and (d,d) states are significantly decreased relative to the corresponding vertical absorption energies, particularly that of the 1^3B_{1g} (d_{z^2},$d_{x^2-y^2}$) (0.28 eV). This fits in with the relaxed geometry of these states (note that the doubly degenerate 1^3E_g state Jahn−Teller (JT) distorts into a "rectangular",[36,37] D_{2h} structure), showing significant changes with respect to the ground-state geometry, as can be seen in Table S1, which collects the optimized geometries of the lowest triplet excited states of NiPc. The relaxed

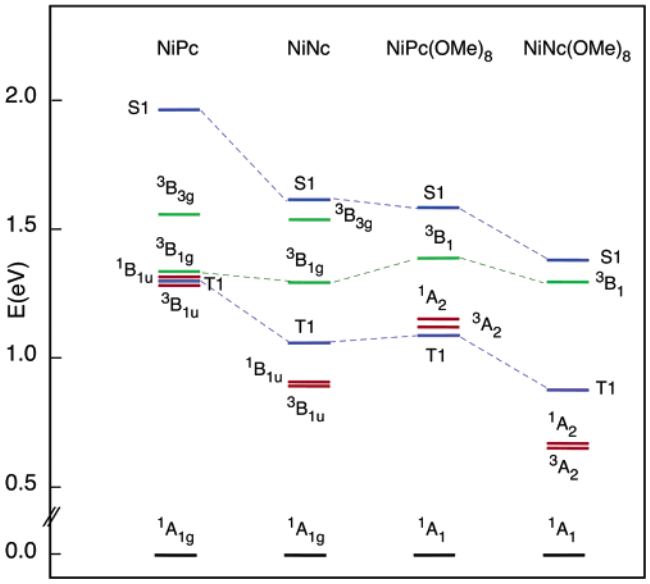

Figure 5. Excited-state diagram for NiPc, NiNc, NiPc(OMe)$_8$, and NiNc(OMe)$_8$. The (d,d) states are indicated with green lines, and LMCT states are indicated with red lines.

geometries of the ^{3}(d,d) and ^{3}LMCT states are characterized by a considerable lengthening of the Ni−N$_p$ distance and a sizable expansion of the macrocycle core. These geometrical changes are directly related to occupation of the $11b_{1g}$, which is a strongly σ-antibonding, Ni−N$_p$ orbital.[29] As for the 1^3E_u (π,π^*) excited state, it JT distorts into a very slightly "stepped" C_{2h} structure. However, as can be inferred from the structural parameters gathered in Table S1, this state fails to show significant geometrical relaxation. Consistent with the minor conformational relaxation, the adiabatic excitation energy of the JT-distorted 1^3A_u (π,π^*) is only 0.07 eV (see Table 3) lower than the vertical absorption energy. Because of the different relaxation, the minima of the relaxed energy surfaces of the 1^3B_{1g} (d_{z^2},$d_{x^2-y^2}$), $1^{1,3}B_{1u}$ (LMCT), and $1^3A_u(\pi,\pi^*)$ (T1 in Figure 5) lie at nearly the same energy. A gap of ∼0.2 eV separates this manifold of excited states from the upper lying 1^3B_{3g} (d_π,$d_{x^2-y^2}$) state (see the excited-state diagram in Figure 5).

According to TDDFT results, other excited states may become involved in the decay of the primary excited $S_1(\pi,\pi^*)$ state, besides the ones just discussed. These are the 1^3A_{2g}, 1^3B_{2g}, and 1^3A_{1g} MLCT states arising from the $6e_g \rightarrow 7e_g$ ($d_\pi \rightarrow \pi^*$) transition, which lie vertically at nearly the same energy as the $S_1(\pi,\pi^*)$. These states are not expected to undergo significant conformational relaxation; therefore, they are likely to intervene only at the very early stage of the $S_1(\pi,\pi^*)$ decay.

The excited-state diagram in Figure 5 clearly indicates that, in substituted NiPcs, the ^{3}(d_{z^2},$d_{x^2-y^2}$), ^{1,3}LMCT, and $T_1(\pi,\pi^*)$ are the most plausible candidates as deactivation channels for the initially excited $S_1(\pi,\pi^*)$ state. The relative energies of these states vary significantly along the series due to the change in the relative position of the Gouterman LUMOs and the unoccupied metal level ($d_{x^2-y^2}$) with respect to the HOMO (see Figure 2). Thus, it can be anticipated that the deactivation pathway of the $S_1(\pi,\pi^*)$ state might differ from one compound to another.

(30) What we call LMCT transitions are not really ligand-to-metal CT transitions, the classification in terms of LMCT used here being merely based on the character of the orbitals involved in the transitions. In fact, a thorough analysis of the changes in Mulliken population accompanying these transitions reveals that no net charge transfer occurs from the ligand to the metal, but only a reorganization of the electronic density occurs, which happens quite frequently in the so-called LMCT states of transition-metal complexes (for an extensive discussion on this topic, see ref 31). Therefore, the well-known failure of TDDFT in predicting the excitation energies of charge-transfer states correctly (see refs 31−35) does not occur here, and the TDDFT energies calculated for the LMCT states can be trusted.
(31) Rosa, A.; Ricciardi, G.; Gritsenko, O.; Baerends, E. J. *Struct. Bonding* **2004**, *112*, 49.
(32) Casida, M. E.; Gutierrez, F.; Guan, J.; Gadea, F.-X.; Salahub, D.; Daudey, J.-P. *J. Chem. Phys.* **2000**, *113*, 7062.
(33) Dreuw, A.; Weisman, J. L.; Head-Gordon, M. *J. Chem. Phys.* **2003**, *119*, 2943.
(34) Dreuw, A.; Head-Gordon, M. *J. Am. Chem. Soc.* **2004**, *126*, 4007.
(35) Gritsenko, O.; Baerends, E. J. *J. Chem. Phys.* **2004**, *112*, 655.
(36) Cory, M. G.; Hirose, H.; Zerner, M. C. *Inorg. Chem.* **1995**, *34*, 2969.
(37) Nguyen, K. A.; Pachter, R. *J. Chem. Phys.* **2003**, *118*, 5802.

The excited-state pattern of NiNc reveals that benzo-annulation of the phthalocyanine ring, while having very little impact on the energy of the ^{3}(d,d) states, causes a downward shift of the $S_1(\pi,\pi^*)$, $T_1(\pi,\pi^*)$, and ^{1,3}LMCT states, resulting from the upshift of the HOMO (Figure 2). The important consequences are that (i) the $^3(d_\pi,d_{x^2-y^2})$ becomes nearly degenerate with the S_1 (it lies adiabatically ~0.1 eV below the S_1) and, hence, might be involved only in the early stage of the deactivation process and (ii) the $^3(d_{z^2},d_{x^2-y^2})$ is no longer degenerate with the $T_1(\pi,\pi^*)$ and ^{1,3}LMCT states. Notably, the ^{1,3}LMCT states undergo a particularly large stabilization; they are actually the lowest excited states due to the concomitant upshift of the HOMO and downward shift of the Ni-$d_{x^2-y^2}$ (see Figure 2).

The upshift of the HOMO results in the downward shift of the $S_1(\pi,\pi^*)$, $T_1(\pi,\pi^*)$, and ^{1,3}LMCT states going from NiPc to its α-methoxy derivative. It is seen that α-methoxy substitution also modifies the energy of the metal states (Figure 5). These $^3(d_\pi,d_{x^2-y^2})$ and $^3(d_{z^2},d_{x^2-y^2})$ lie at a somewhat higher energy in NiPc(OMe)$_8$ than in NiPc and in NiNc, which is caused by the saddling-induced upshift of the Ni-$d_{x^2-y^2}$ orbital. In turn, the ^{1,3}LMCT states end up slightly above the $T_1(\pi,\pi^*)$.

As inferred from the excited-state diagram in Figure 5, the most conspicuous effect of α-methoxy substitution of the Nc ring is the stabilization of the $S_1(\pi,\pi^*)$, $T_1(\pi,\pi^*)$, and ^{1,3}LMCT states, resulting from the upshift of the HOMO going from NiNc to NiNc(OMe)$_8$ (see Figure 2). It is worth noting that, owing to the huge downward shift of the $S_1(\pi,\pi^*)$ in NiNc(OMe)$_8$, the minimum of the relaxed energy surface of the $^3(d_{z^2},d_{x^2-y^2})$ is located immediately below this state and, hence, is expected to play a role, if any, only at the early stage of the deactivation mechanism. Just as in NiPc(OMe)$_8$, the $^3(d_\pi,d_{x^2-y^2})$ lies vertically well above the $S_1(\pi,\pi^*)$. Therefore, even though the relaxation energy would be considered, it is unlikely that this state might play a role in the deactivation of the $S_1(\pi,\pi^*)$.

C. Photophysics. 1. Transient Absorption Experiments: Spectral Observations and Dynamic Properties. Photoexcitation experiments were carried out for all members of the series except NiNc, which had insufficient solubility in all solvents, thus prohibiting the recording of useful transient absorption data.

1.a. NiPc. The excited-state deactivation mechanism of NiPc has not been fully studied heretofore. An early investigation of the excited-state dynamics of NiPc by Millard and Green[38] reported only the relaxation of the first excited singlet state, with a lifetime of 2.8 ps. These authors suggested that the S_1 state decayed to "a variety of possible states of different spin multiplicity".[38] Their single probe wavelength measurements were unable to detect intermediate species involved in the deactivation sequence. To clarify this issue, transient absorption experiments with excitation at 625 nm were carried out on NiPc (20 μM) in 1-chloronaphthalene, a noncoordinating solvent in which the complex shows acceptable solubility. Figure 6 shows spectral profiles at a series of delay times after 625 nm excitation. The earliest time spectrum in Figure 6 shows no indication of significant positive absorption in the spectral region at the blue side of the ground-state Q bands. This is markedly different from the situation with NiPc(OBu)$_8$[10] (also see Figure 7) and other MPc and MNc systems[6,15,16] where absorptions at the blue

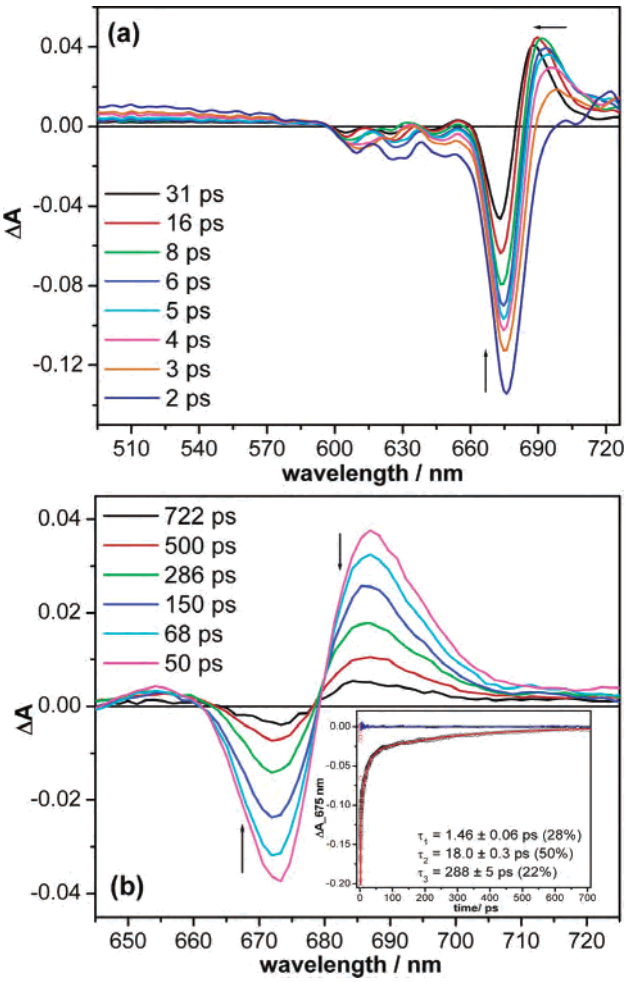

Figure 6. Transient absorption behavior of NiPc in 1-chloronaphthalene solution photoexcited at 625 nm. (a) Cooling of the vibrationally hot (d,d) state; (b) decay of the (d,d) state. Inset: kinetic profile at 675 nm.

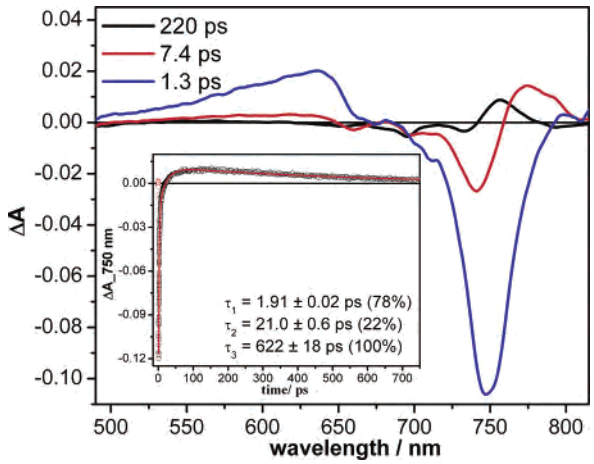

Figure 7. Transient absorption spectra of NiPc(OBu)$_8$ in 1-chloronaphthalene photoexcited at 625 nm corresponding to three species participating in the deactivation pathway. Inset: time profile at 750 nm.

(38) Millard, R. R.; Green, B. I. *J. Phys. Chem.* **1985**, *89*, 2976.

side of the Q bands have been assigned to transitions localized on the respective π systems, namely, $S_1 \rightarrow S_n$ or $T_1 \rightarrow T_n$. Thus, the first observed transient (FOT) is, most likely, not the $S_1(\pi,\pi^*)$ state. The earliest time transient absorption spectra (Figure 6a) have an asymmetric derivative-like shape and experience a blue shift with time, finally evolving at 31 ps to a spectrum having symmetric derivative-like shape (the 50 ps spectrum in Figure 6b). This latter is typical of a "classic" (d,d) state spectrum, as observed in nominally planar nickel porphyrins,[39−41] NiOMTP (OMTP = octamethylthioporphyrin),[42] and NiPc(OBu)$_8$.[10] The blue shift and spectral narrowing of the early spectral feature have been previously observed in other nickel tetrapyrrole systems[10,39−43] and have been ascribed to vibrational relaxation and conformational readjustment within the state. In NiPc, this cooling shows biphasic kinetics (Figure 6b, inset); the fast process with a 1.4 ps lifetime is probably relaxation within the molecule (IVR), whereas the slower one ($\tau \sim 18$ ps) represents thermal losses to solvent oscillators. After vibrational cooling, the (d,d) state deactivates to the ground state, as shown by isosbestic behavior at 680 nm (Figure 6b), with a lifetime of 300 ps.

1.b. NiPc(OBu)$_8$. For the sake of comparison with NiPc, the photophysical behavior of NiPc(OBu)$_8$ has been reinvestigated in 1-chloronaphthalene. Figure 7 shows three spectral profiles taken at different post-pulse delays after 625 nm excitation. Comparison with previous results in toluene[10] reveals that the spectral and temporal characteristics are substantially the same as those in toluene.

1.c. NiNc(OBu)$_8$. Ultrafast pump−probe absorption spectrometry employing excitation wavelengths of 330 (B band), 845 (Q-band maximum), and 800 (vibrational peak of the Q band) nm was used to investigate the excited-state behavior of NiNc(OBu)$_8$. The transient species formed were probed in the visible and near-IR region of the spectrum. Ultrafast experiments were conducted either in toluene or in 1-chloronaphthalene. As no significant solvent effect was detected, only the results obtained in toluene are here reported and discussed. Figure 8 shows overlaid transient absorption spectra recorded at different delay times after excitation of NiNc(OBu)$_8$ with 800 nm pulses. Figure 9 shows transient absorption spectra of the excited-state species probed in the near-IR region. No dependence of the transient spectral and temporal characteristics on excitation wavelength was observed.

The spectral feature formed within the instrument response time (ca. 200 fs) is characteristic of excited states localized on the π system of phthalocyanine and naphthalocyanine macrocycles,[6,10,15,16,44−47] namely, a broad positive absorption

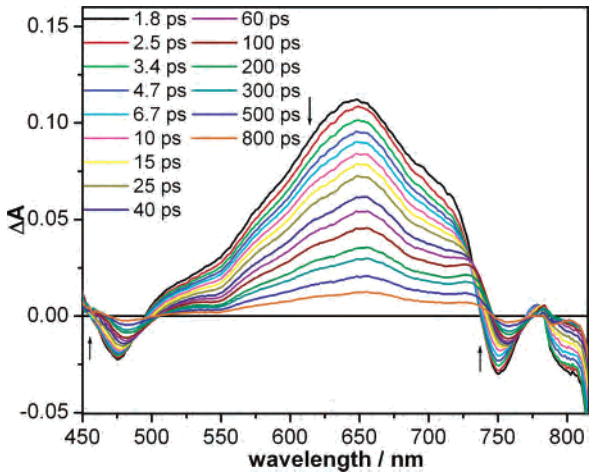

Figure 8. Evolution of the transient absorption spectra of NiNc(OBu)$_8$ in toluene (ca. 30 μM). The energy of the pump was 6 μJ/pulse.

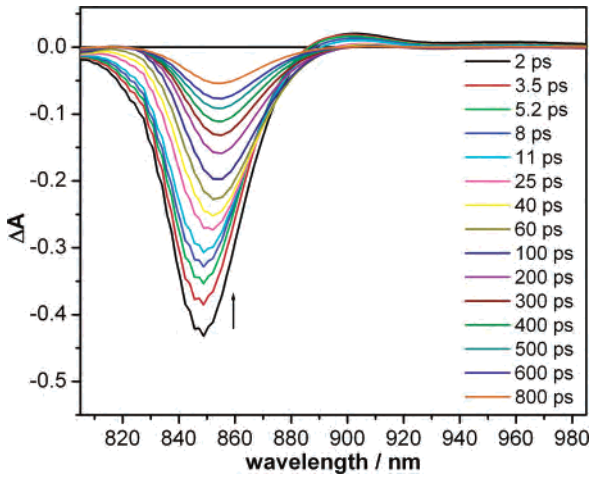

Figure 9. Transient absorption spectra of NiNc(OBu)$_8$ in toluene photoexcited at 800 nm in near-IR region. The energy of the pump was 5 μJ/pulse.

with a maximum at 650 nm and two negative bands at 475 and 750 nm due to the ground-state depopulation.

The transient absorption spectra in the near-IR region (Figure 9) were dominated by a strong negative absorption band due to the ground-state depopulation in the region of the ground-state Q-band maximum, with a small positive absorption band to the red at around 900 nm. Figure 10 shows the temporal profiles of the transient absorption displayed by NiNc(OBu)$_8$ taken at four spectral regions. The decay of the positive absorption signal as well as the recovery of the negative signal were well-fitted by a three-exponential function to a zero baseline, providing three lifetimes.

Table S4 summarizes the kinetic data for probe wavelengths ranging from 475 to 920 nm for the compound. As can be inferred from this table, the lifetime of the fastest component and its relative contribution to the overall decay showed strong wavelength dependence, varying from ca. 0.3

(39) Rodriguez, J.; Holten, D. *J. Chem. Phys.* **1989**, *91*, 3525.
(40) Rodriguez, J.; Kirmaier, C.; Holten, D. *J. Am. Chem. Soc.* **1989**, *111*, 6500.
(41) Rodriguez, J.; Kirmaier, C.; Holten, D. *J. Chem. Phys.* **1991**, *94*, 6020.
(42) Rosa, A.; Ricciardi, G.; Baerends, E. J.; Zimin, M.; Rodgers, M. A. J.; Matsumoto, S.; Ono, N. *Inorg. Chem.* **2005**, *44*, 6609.
(43) Drain, C. M.; Kirmaier, C.; Medforth, C. J.; Nurco, D. J.; Smith, K. M.; Holten, D. *J. Phys. Chem.* **1996**, *100*, 11984.
(44) Gunaratne, T. C.; Kennedy, V. O.; Kenney, M. E.; Rodgers, M. A. J. *J. Phys. Chem. A* **2004**, *108*, 2576.
(45) Fournier, M.; Pepin, C.; Houde, D.; Ouellet, R.; van Lier, J. E. *Photochem. Photobiol. Sci.* **2004**, *3*, 120.
(46) Aoudia, M.; Cheng, G.; Kennedy, V. O.; Kenney, M. E.; Rodgers, M. A. J. *J. Am. Chem. Soc.* **1997**, *119*, 6029.
(47) Firey, P. A.; Ford, W. E.; Sounik, J. R.; Kenney, M. E.; Rodgers, M. A. J. *J. Am. Chem. Soc.* **1988**, *110*, 7626.

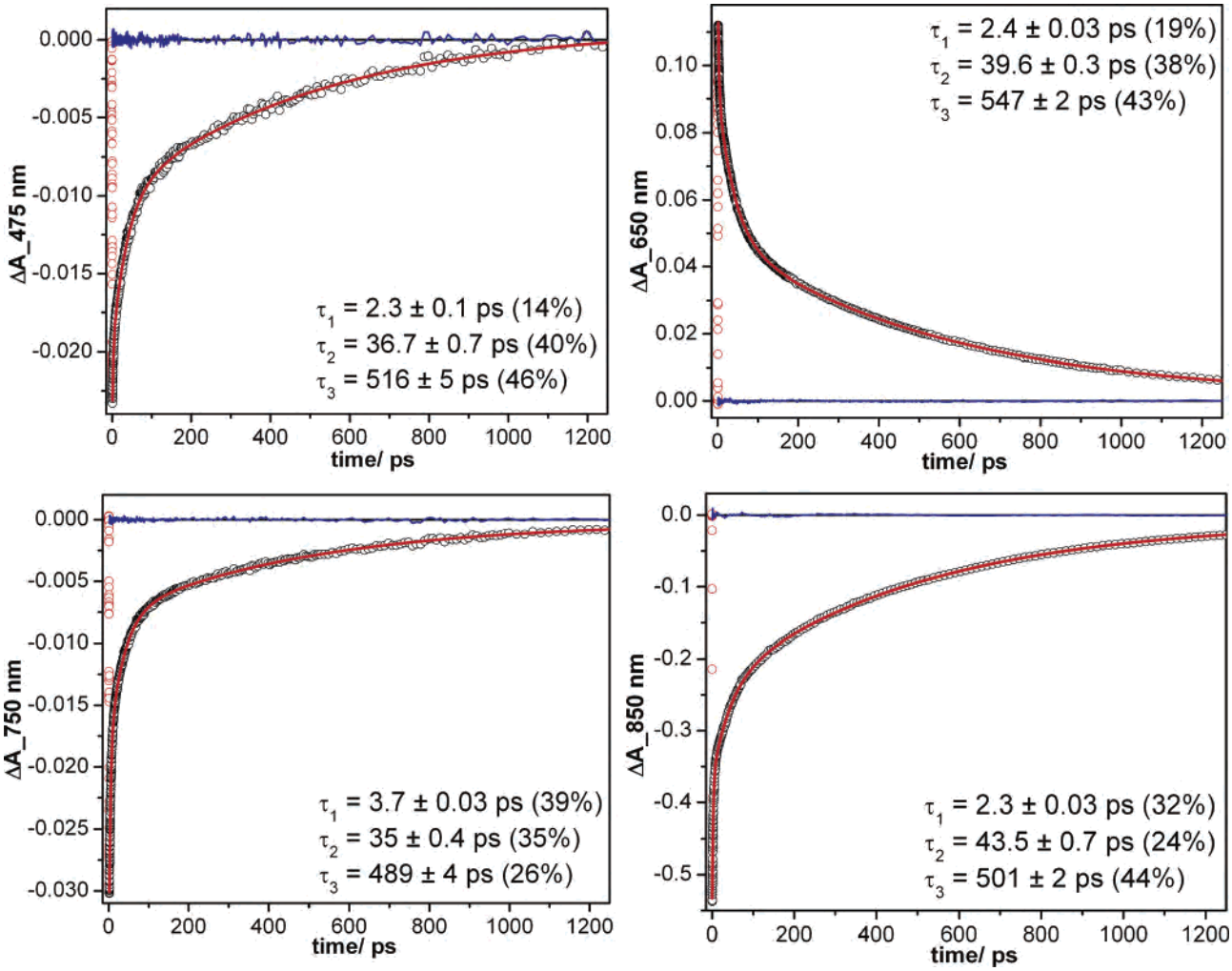

Figure 10. Kinetic profiles of the transient absorption signal at various probe wavelengths for $NiNc(OBu)_8$ in toluene after photoexcitation at 800 nm.

to ca. 3.5 ps. A plot of this first lifetime versus wavelength is shown in Figure 11.

The intermediate lifetime, although longer, showed a similar wavelength dependence (Table S4); the slowest lifetime component was essentially wavelength independent at ca. 500 ps. Figure 12 illustrates the kinetic behavior of the transient absorption at 730 nm, where a characteristic spectral shoulder arises at later delay times.

2. Interpretation of the Photophysical Behavior. The experimental and theoretical results described previously can be employed to elucidate the dynamics of the excited states of the compounds studied and to comment on the separate and combined effects of α-butoxy substitution and benzo-annulation. The photophysical behavior of $NiNc(OBu)_8$, not reported before, will be considered first.

2.a. The Photophysical Behavior of $NiNc(OBu)_8$. The salient features of the transient spectra observed immediately after pump−probe excitation of $NiNc(OBu)_8$ are as shown in Figure 8. There is a broad, almost featureless positive ΔA region stretching from ca. 500 to ca. 740 nm, with negative ΔA regions outside this range. During the first 15 ps or so, the regions of negative ΔA underwent slight spectral shifts to the red, after which no further shifting was observed. Throughout the spectral range, it was necessary to use a three-exponential expression to obtain satisfactory fits to the time profiles. The main positive absorption band, $\lambda_{max} = 650$ nm, decayed with minimal spectral changes, save for the development of a poorly resolved peak at 730 nm on the red side of the major absorption band. Leaving aside a consideration of the very early, wavelength-dependent kinetic component for the moment, what is observed is that the absorption growth at 730 nm has a similar lifetime to the second decay component at shorter wavelengths. This suggests that the 730 nm species is generated from the 650 nm transient. However, it is clearly not a simple situation because, having been produced, the 730 nm species decays to the baseline with the same lifetime as observed for the third component of the decay at all other wavelengths, indicating that the two species have a common lifetime. This can be understood if the 730 and 650 nm transients are in dynamic equilibrium, and the 19 ps growth lifetime is the rate at which the equilibrium is established, and the 500 ps decay, at all wavelengths, is the decay of the equilibrium state. A major requirement for the equilibrium condition is that the two states participating are close in energy. Turning to Table 4, it is seen that candidate states for satisfying this condition are the 1^3B_2 (π,π^*) and the nearly degenerate $^{1,3}A_2$ (LMCT) pair. Although the calculated energy difference is

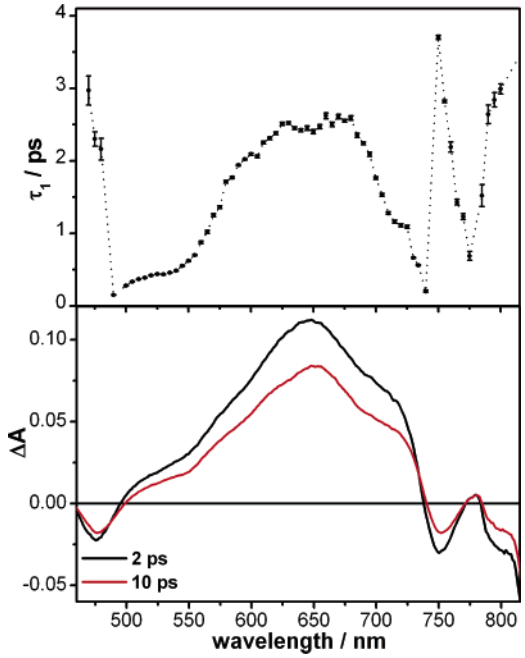

Figure 11. Upper panel: first lifetime/wavelength dependence. Lower panel: two transient absorption spectral cuts taken at 2 and 10 ps for NiNc-$(OBu)_8$ in toluene.

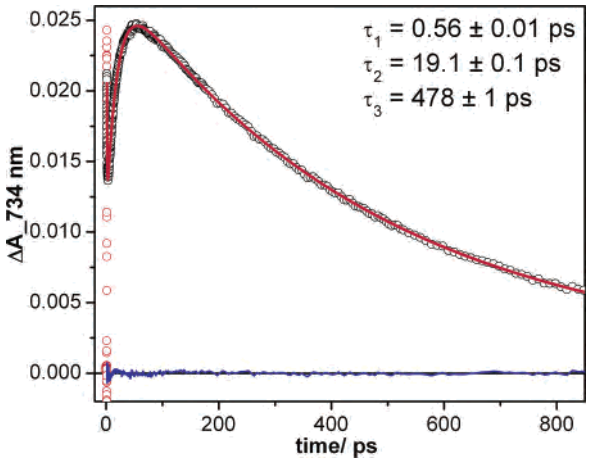

Figure 12. Kinetic profiles of the transient absorption signal at 730 nm for NiNc$(OBu)_8$ in toluene after photoexcitation at 800 nm.

~0.2 eV, there is enough uncertainty in the calculations for the states to be actually closer than this.

Taking as a working hypothesis that the FOT (650 nm) is the 1^3B_2 (π,π^*) state and the 730 nm daughter is one of the $^{1,3}A_2$ (LMCT) pair, and that the two are in a dynamic equilibrium, it is instructive to seek other evidence. First, unlike the case of NiPc$(OMe)_8$, the $^3B_2$ (d_{z^2},$d_{x^2-y^2}$) state has a calculated energy that is too high for it to be involved in the deactivation of the $S_1(\pi,\pi^*)$ state produced by excitation in the Q band. Moreover, no tell-tale absorption pattern of a (d,d) state was seen in the experimental spectra (see, e.g., the NiPc spectra in Figure 6). The spectral shape of the FOT, namely, a broad positive absorption at around 650 nm, is reminiscent of the transient absorption signal arising from the $T_1 \rightarrow T_n$ transition of the Pd(II)-octabutoxynaphthalocyanine studied earlier.[6] The Pd analogue, however, has a triplet lifetime of hundreds of nanoseconds and showed phosphorescence emission at 0.93 eV.[6] In addition, TDDFT results on PdNc$(OMe)_8$ allocated $T_1(\pi,\pi^*)$ vertically at 0.95 eV,[48] almost isoenergetic with that for $T_1(\pi,\pi^*)$ in NiNc-$(OBu)_8$, calculated here to be 0.92 eV (Table 4). Taking this energy argument into account, it would not be unreasonable to conclude that the behavior of the $^3(\pi,\pi^*)$ in NiNc$(OBu)_8$ would be similar to that exhibited by the Pd complex. However, the value of the 500 ps lifetime measured here for the decay of the 650 nm transient in NiNc$(OBu)_8$ seems much too short for the spin-forbidden repopulation of the ground state from the π-localized triplet excited state, and only electronic factors, involving metal orbitals, that are missing in the Pd complex can explain the short $T_1(\pi,\pi^*)$ lifetime. Indeed, in NiNc$(OBu)_8$, the proximity of the LMCT and the $T_1(\pi,\pi^*)$ states, as predicted by the calculations, supports the proposal that these states are in dynamic equilibrium, allowing an understanding of why the lifetime is less than expected. Under conditions where the reactions participating in the equilibrium are proceeding much more rapidly than the decays of the individual participating states, the lifetime of the equilibrium state is a linear combination of the two individual lifetimes, weighted by the mole fraction contributions of each.[49]

In summary, it is considered most likely that photoexcitation within the Q band of NiNc$(OBu)_8$ generates the 1^1E (π,π^*) state, which converts to the $^3(\pi,\pi^*)$ state within the instrument response time (ca. 200 fs). This π-localized triplet state in our experiment is seen as the first observed transient (FOT). This state rapidly (ca. 19 ps lifetime) and reversibly converts into the ^{3}LMCT or the ^{1}LMCT state, and the equilibrium state, so generated, decays to the ground state with a lifetime of ca. 500 ps. That the intersystem crossing (ISC) process $1^1E \rightarrow 1^3E$ (1^3B_2) occurs so rapidly (within the instrument response time) is certainly highly unusual; metallophthalocyanines with p-block metal centers show ISC rate constants in the 1 ns^{-1} range.[16,44] The most likely explanation of this is that ISC is facilitated by the 1^3B_2 (d_{z^2},$d_{x^2-y^2}$) state. This state has, indeed, a calculated adiabatic energy of 1.31 eV, some 70 meV above the 1^1E (Q) state. Such an energy difference is within the confidence limits of the calculations, and it is not unlikely that these states are close to degenerate and, thus, interact strongly, providing fast intersystem crossing.

Returning to the kinetic data, we have argued that the second and third exponential components correspond, respectively, to the conversion of the $^3(\pi,\pi^*)$ to the ^{3}LMCT or ^{1}LMCT state and to the latter's decay to the ground state; it remains to consider the earliest component. Considering that the FOT is identified as the $T_1(\pi,\pi^*)$ that must be formed very rapidly from $S_1(\pi,\pi^*)$, it must initially carry excess vibrational energy, and given that the spectral shape did not change during this decay event, it is not unreasonable to assign the first exponential component to the cooling of the state. In NiNc$(OBu)_8$, the first and second decay components

(48) Soldatova, A. V.; Kim, J.; Rosa, A.; Ricciardi, G.; Kenney, M. E.; Rodgers, M. A. J. Manuscript in preparation.
(49) Birks, J. B. *Photophysics of Aromatic Molecules*; Wiley: London, 1970.

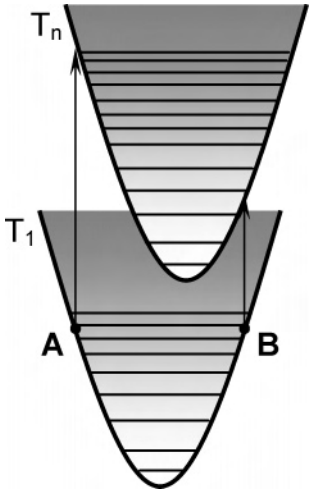

Figure 13. A schematic explanation of the wavelength dependence of the first lifetime (see text).

showed significant wavelength dependence (see Figure 11 for the early component). Interestingly, as the figure shows, at the two crossings between regions of negative and positive absorption, the decay lifetimes are shortest; in the region between, the dependence is bell shaped. This can be understood as a manifestation of intramolecular vibrational relaxation from high-lying vibrational quantum states where the wave functions are such that the oscillators have a high probability of being near the classical turning points.[50] The reason for the bell-shaped nature of the lifetime wavelength dependence (Figure 11) must arise from the detailed nature of the upper and lower potential energy surfaces, and a simplistic schematic explanation is presented in Figure 13. There, it is seen that upper and lower electronic curves are drawn to be slightly offset, such that upward transitions from the two turning points, labeled A and B, occur at different energies and correspond to the two lifetime minima in Figure 11. It is likely that a similar explanation holds for the second temporal component.

2.b. Effects of the Octabutoxy Substitution and Benzoannulation on the Deactivation of the Excited States. A comparison of the photophysical behaviors of NiPc and NiPc(OBu)$_8$ allows the effects of octabutoxy substitution to be understood. In the report on the relaxation of the NiPc(OBu)$_8$ excited states,[10] the experimental and theoretical results have shown that the S_1 state, generated upon photoexcitation into the Q band, deactivates through the $^3(d_{z^2},d_{x^2-y^2})$ state, which in turn, converts to the ^{3}LMCT state that finally repopulates the ground-state surface. Figure 7 represents time-resolved absorption data for NiPc(OBu)$_8$ in a 1-chloronaphthalene solution, where the three spectral signatures of the S_1 (1.3 ps), $^3(d_{z^2},d_{x^2-y^2})$ (7.4 ps), and ^{3}LMCT states (220 ps) are closely similar to those observed in toluene solution.[10] However, in the case of NiPc (Figure 6), the deactivation pathway appears to be quite different, allowing an interesting comparison to be drawn between the early processes in deactivation of the S_1 states of NiPc and NiPc(OBu)$_8$. The octabutoxy derivative (Figure 7) shows clear evidence of a $S_1 \rightarrow S_n$ transition in the 600 nm region with a lifetime of 1.9 ps; the unsubstituted compound shows no such spectral evidence. In fact, the FOT is a hot (d,d) state. Thus, NiPc, as NiNc(OBu)$_8$ considered previously, exhibits an ultrafast ISC process out of the photogenerated Q state, probably induced by the proximity of the 1^3A_{1g} MLCT state. The TDDFT results presented in Table 3 indicate that the next state below is the 1^3E_g $(d_\pi,d_{x^2-y^2})$ state, lying adiabatically at 1.56 eV. Below this state, there are four states lying adiabatically very close in energy, namely, the $^3(d_{z^2},d_{x^2-y^2})$ state at 1.34 eV, the nearly degenerate $1^{1,3}B_{1u}$ LMCT pair close to 1.30 eV, and the 1^3A_u (π,π^*) at 1.30 eV. It must be stated, however, that the ordering of these states may differ on account of the uncertainty in the calculated energies. What is clear from the experimental data is that the state that precedes the recovery to the ground-state surface is a cooled (d,d) state, and the lowest-lying of these (Table 3) is the 1^3B_{1g} $(d_{z^2},d_{x^2-y^2})$. In all likelihood then, the immediate precursor of the ground state is the 1^3B_{1g} state with a lifetime of some 300 ps, similar to that of ^{3}(d,d) states in some Ni porphyrins.[39−42] Whether a vibrationally hot version of this state, or a hot 1^3E_g state, is the one that is observed as the FOT is not clear. Both of these states, being of (d,d) nature, will have absorption spectra that are dominated by the π system and only affected in a minor way by the metal electronic configuration. The UV−vis transient absorption spectra in Figure 6 are insufficiently detailed to provide a resolution of this question.

The large destabilization of the HOMO in NiPc(OMe)$_8$ due to an antibonding interaction with the oxygen lone pairs considerably lowers the energy of the LMCT states, removing their quasidegeneracy with the $^3(d_{z^2},d_{x^2-y^2})$ state that occurs in NiPc. This makes possible the population of the ^{3}LMCT state observed in the transient absorption experiment.

Concerning the effect of the benzoannulation of the Pc ring on the deactivation of the $S_1(\pi,\pi^*)$, we are not able to draw definitive conclusions, as insufficient solubility of NiNc in noncoordinating solvents prevented us from obtaining transient absorption data on this compound. However, on the basis of TDDFT calculations and transient absorption data obtained for NiNc(OBu)$_8$, some projections can be made. For example, the $^3(d_{z^2},d_{x^2-y^2})$ does not appear in photoexcited NiNc(OBu)$_8$ during the ultrafast transient absorption experiment because of its near-degeneracy with the S_1 state. Nevertheless, it might play a more distinct role in the excited-state deactivation in the NiNc complex since, in that complex, this near-degeneracy is removed (Figure 5), and the energy gap between S_1 and the (d,d) state is more like that in the NiPc(OBu)$_8$ complex, where the (d,d) state was evident. Moreover, both the $T_1(\pi,\pi^*)$ and ^{3}LMCT$(\pi,d_{x^2-y^2})$

(50) The optical absorption spectrum of an excited vibronic state arises from the sum of all possible Franck−Condon transitions to vibrational levels in a higher electronic state. When the origin state is vibrationally cold, transitions originating at the equilibrium geometry are favored because the wave function has maximum amplitude there. However, when the origin state is hot, upward transitions originating closer to the classical turning points become increasingly probable. By their very nature, the vibrational states with high quantum numbers have a higher density of vibrational oscillators below them than do states with lower quantum numbers, and they will therefore cool faster, resulting in different wavelength regions having different cooling lifetimes, as observed here.

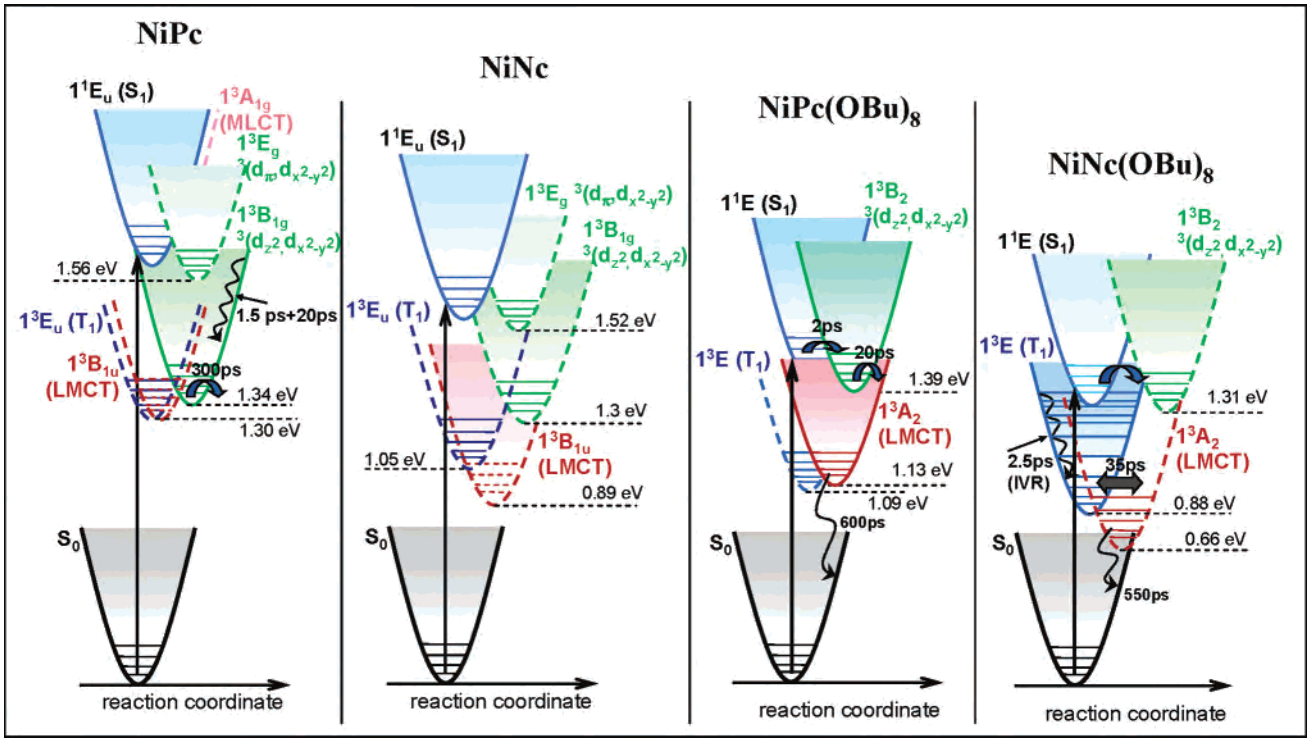

Figure 14. Proposed schematic diagrams for the excited-state relaxation pathways of NiPc, NiNc, NiPc(OBu)$_8$, and NiNc(OBu)$_8$ in 1-chloronaphthalene.

would most likely play a role in the deactivation mechanism, as in the case in NiNc(OBu)$_8$.

Figure 14 concisely summarizes the photophysical properties of the metallotetrapyrroles investigated herein.

Conclusions

The excited-state spectral and dynamic behavior of NiNc(OBu)$_8$, a very promising photothermal sensitizer, has been investigated by ultrafast transient absorption spectrometry and interpreted in light of DFT/TDDFT theoretical studies. It is found that the initially formed $S_1(\pi,\pi^*)$ state deactivates, within the time resolution of the instrument (200 fs), to the vibrationally hot $T_1(\pi,\pi^*)$ state. The quasidegeneracy of the $S_1(\pi,\pi^*)$ and $^3(d_{z^2},d_{x^2-y^2})$ allows for fast intersystem crossing to occur. After vibrational relaxation (ca. 2.5 ps), the $T_1(\pi,\pi^*)$ converts rapidly (ca. 19 ps lifetime) and reversibly into the ^{3}LMCT$(\pi,d_{x^2-y^2})$ state. The so generated equilibrium state decays to the ground state with a lifetime of ca. 500 ps.

With the aim to independently characterize the impact of α-octabutoxy substitution and benzoannulation of the phthalocyanine ring on the deactivation pathway of the $S_1(\pi,\pi^*)$ state, the ground- and excited-state properties and the photophysical behavior of NiPc, NiNc, and NiPc(OBu)$_8$ have also been examined. Ultrafast experiments and DFT/TDDFT calculations have consistently shown that peripheral substitution of the Pc ring modifies the photodeactivation mechanism of the $S_1(\pi,\pi^*)$ by inducing substantial changes in the relative energies of the $S_1(\pi,\pi^*)$, $^3(d_\pi,d_{x^2-y^2})$, $^3(d_{z^2},d_{x^2-y^2})$, $T_1(\pi,\pi^*)$, and ^{1,3}LMCT$(\pi,d_{x^2-y^2})$ excited states. The actual position of these states has been found to markedly depend on the location of the Gouterman LUMOs and the unoccupied metal level $(d_{x^2-y^2})$ with respect to the HOMO. In NiPc, the $S_1(\pi,\pi^*)$ state undergoes ultrafast (<200 fs) ISC into a hot ^{3}(d,d) state, which cools within 20 ps. This cooled (d,d) state, probably 1^3B_{1g} $(d_{z^2},d_{x^2-y^2})$, repopulates the ground state with a lifetime of 300 ps.

Previous and present results for NiPc(OBu)$_8$ indicate that, in this complex, the $S_1(\pi,\pi^*)$ state deactivates through the $^3(d_{z^2},d_{x^2-y^2})$, which is no longer degenerate with the $T_1(\pi,\pi^*)$ and ^{1,3}LMCT$(\pi,d_{x^2-y^2})$. The $^3(d_{z^2},d_{x^2-y^2})$, in turn, converts to the ^{3}LMCT$(\pi,d_{x^2-y^2})$, which finally repopulates the ground-state surface within 640 ps. Insufficient solubility of NiNc in noncoordinating solvents prevented us from obtaining transient absorption data. However, on the basis of TDDFT calculations and transient absorption data obtained for NiNc(OBu)$_8$, it can be anticipated that (i) the $^3(d_{z^2},d_{x^2-y^2})$ that does not appear spectroscopically during the ultrafast transient absorption experiment in the NiNc(OBu)$_8$ complex due to its near-degeneracy with the S_1 state might participate in the excited-state deactivation in NiNc and (ii) both the $T_1(\pi,\pi^*)$ and ^{3}LMCT$(\pi,d_{x^2-y^2})$ states are likely to play a role in the deactivation mechanism.

In this study, toluene and chloronaphthalene have been employed as solvents to avoid coordinating reactions at the metal site. It can be questioned as to whether this is a relevant model medium for biological media. The compounds are exceedingly lipophillic, and in cellular and tissue studies, they are necessarily administered via liposomes.[10] In vivo, the compounds reside in hydrophobic organelles, and for this reason, it would appear that toluene can be regarded as a not-inappropriate environment for photophysical studies.

The work described here lends credence to the argument that a comprehensive understanding of the deactivation mechanisms of metallotetrapyrrole excited states, particularly when the metal is a first-row transition metal, can only be properly gained when the natures and energies of the

spectroscopically silent states lying between the photogenerated state and the ground state are known. Such information is available only through theoretical approaches, and this report adds to the growing evidence[10,27,42,51] that the combination of DFT and TDDFT is capable of achieving considerable accuracy in excitation energy calculations for large molecules such as MTPs. This knowledge of the nature and energies of the low-lying excited states along the relaxation pathways has proven extremely useful for interpreting the results of transient absorption experiments and to assist in understanding the differences in the observed deactivation rates from compound to compound.[10,42]

Acknowledgment. The photophysical studies conducted at the Ohio Laboratory for Kinetic Spectrometry (BGSU) were supported, in part, by NIH Grant CA 91027 and by an instrumentation grant from the Hayes Investment Foundation (Ohio Board of Regents). A.V.S. thanks the McMaster Foundation at BGSU for a predoctoral fellowship. A.R. and G.R. wish to thank the Italian MIUR (Ministero dell' Istruzione, dell' Università e della Ricerca) and the Università della Basilicata, Italy, for a grant (Grant 2003038084_002). Grateful thanks are expressed to Dr. Eugene Danilov for the technical assistance with ultrafast instrumentation.

Supporting Information Available: Optimized geometrical parameters for the lowest triplet excited states of NiPc, NiNc, and $NiNc(OMe)_8$ (Tables S1−S3). Lifetimes and relative amplitudes of the transient absorption dynamics of $NiNc(OBu)_8$ in toluene after 800 nm excitation (Table S4). This material is available free of charge via the Internet at http://pubs.acs.org.

IC061524O

(51) Rogers, J. E.; Nguyen, K. A.; Hufnagle, D. C.; McLean, D. G.; Su, W.; Gossett, K. M.; Burke, A. R.; Vinogradov, S. A.; Pachter, R.; Fleitz, P. A. *J. Phys. Chem. A* **2003**, *107*, 11331.